Available online at www.sciencedirect.com
ScienceDirect
Polymer 48 (2007) 1367–1378
polymer
www.elsevier.com/locate/polymer

Experimental studies and molecular modelling of the stress–optical and stress–strain behaviour of poly(ethylene terephthalate). Part II: Molecular modelling of birefringence of poly(ethylene terephthalate) networks

J.I. Cail [a], R.F.T. Stepto [a,*], I.M. Ward [b]

[a] Polymer Science and Technology Group, School of Materials, The University of Manchester, Grosvenor Street, Manchester M1 7HS, UK
[b] IRC in Polymer Science and Technology, School of Physics and Astronomy, University of Leeds, Leeds LS2 9JT, UK

Received 9 September 2006; received in revised form 18 December 2006; accepted 31 December 2006
Available online 23 January 2007

Abstract

The Monte-Carlo (MC) approach of Paper I is developed to predict the birefringence of PET. An extension of the modelling of polarisability is used that accounts for chain flexibility and for structural units containing several types of bonds. The rotational-isomeric-state (RIS) model for PET chains in melts is employed to calculate the polarisability of the terephthaloyl segment and of each of the 27 possible conformations of the five skeletal bonds of the glycol segment. These polarisabilities then enable the birefringent properties of drawn PET melts to be predicted. A method of pre-averaging the individual glycol polarisabilities that greatly reduces the length of the calculation is shown to be valid.

It is found that shorter PET chains produce higher values of birefringence ($\Delta\tilde{n}$) for a given deformation. This trend is due to greater proportions of the chains reaching higher conformational extensions and therefore becoming more oriented. In disagreement with Kuhn and Grün theory, $\Delta\tilde{n}$ is not linearly related to $\lambda^2 - \lambda^{-1}$. This non-linear behaviour is related to the non-linear behaviour of the orientation functions of the terephthaloyl and glycol segments, $\langle P_2(\cos\zeta_{ter})\rangle$ and $\langle P_2(\cos\zeta_{gly})\rangle$, with $\lambda^2 - \lambda^{-1}$. The non-linear behaviour of $\langle P_2(\cos\zeta_{ter})\rangle$ with $\lambda^2 - \lambda^{-1}$ was confirmed experimentally in Paper I, where the measured values of $\langle P_2(\cos\zeta_{ter})\rangle$ were found to be closely predicted by the present MC modelling.

In the present paper, the predicted values of $\Delta\tilde{n}$, calculated according to various published values of bond polarisabilities are presented and discussed. They will be used in Paper III to model the measured birefringence of drawn PET.

Keywords: Poly(ethylene terephthalate); Birefringence; Monte-Carlo modelling

1. Introduction

An amorphous polymer-network material is usually optically isotropic as its chains are randomly oriented. It is therefore characterised by a single value of refractive index, $\tilde{n}$, irrespective of the direction of the incident light used. However, if such a material is subjected to a macroscopic strain, molecular orientation develops and the material may begin to show anisotropic properties, including optical anisotropy or birefringence.

The photoelastic properties of elastomeric networks received particular attention in the period 1945–1970, due to the studies of Treloar, Saunders, Gent and their collaborators on rubbers and crosslinked polyethenes. The starting point for an understanding of the development of optical anisotropy with strain was the 1942-theory of Kuhn and Grün [1]. This theory replaces the true molecular network by an idealised network of ν identical Gaussian chains, each of which consists of m freely-jointed links of length l'. They are equivalent random links in that any valence-angle and conformational restrictions are accounted for by matching the dimensions of this hypothetical chain with those of a real chain. The dimensions usually chosen are the mean-square end-to-end distance $\left(\langle r^2\rangle\right)$

* Corresponding author. Tel./fax: +44 1625 872581.
E-mail address: rfts@tesco.net (R.F.T. Stepto).

0032-3861/$ - see front matter © 2007 Elsevier Ltd. All rights reserved.
doi:10.1016/j.polymer.2006.12.049

and the fully-extended chain length (r_{max}). For strains that are not too large, the Kuhn and Grün theory shows that both birefringence, $\Delta\tilde{n}$, and true stress, t, are proportional to $\lambda^2 - \lambda^{-1}$, where λ is the deformation ratio. Hence, there is a constant stress–optical coefficient, C, where

$$C = \frac{\Delta\tilde{n}}{t} \tag{1}$$

It was soon recognised that the Gaussian network model was inadequate because, even at comparatively modest deformation ratios, the stress–optical coefficient, as defined by Eq. (1), was not a constant. Early attempts to deal with this issue on the basis of the inverse Langevin function have been well described by Treloar [2] and by Saunders [3]. These studies left some major issues unresolved, partly due to uncertainties in predicting accurate values for bond polarisabilities and partly due to uncertainties in dealing with the issue of some chains in a network becoming fully extended.

Pinnock and Ward [4] undertook stress–optical measurements to gain an understanding of the molecular mechanism of the deformation of poly(ethylene terephthalate) (PET) and used the Kuhn and Grün theory for deformation in the rubbery state. The equivalent random-link model for PET did suggest that in tensile drawing a substantial proportion of the molecular chains becomes fully extended at comparatively low draw ratios [5]. In an extension of this work by Nobbs and Bower [6], it was proposed that fully-extended chains rotated according to the affine deformation scheme, but any changes in the lengths of the rotating vector lines were ignored. This process has been called pseudo-affine deformation [7] and corresponds to that proposed by Kratky [8] for the orientation of crystals in semi-crystalline polymers.

In the present paper, the Monte-Carlo (MC) approach of the preceding paper [9] is used to predict the birefringence of PET. This approach has previously been successfully applied to predict the network stress–strain properties of polyethylene (PE) and poly(dimethyl siloxane) (PDMS) [10,11], and to predict the stress–optical properties of PE [12,13], where it was shown that the Kuhn and Grün theory is quantitatively incorrect.

The prediction of $\Delta\tilde{n}$ for PET needs an extension to the MC modelling of polarisability to include chain flexibility and structural units containing several different types of bonds. In previous papers [4,14,15] it has been assumed that it is adequate to consider that a whole PET repeat unit becomes aligned with no account being taken of changes in skeletal-bond conformations during stretching. This assumption is clearly inadequate and in the present paper the PET molecules are regarded as aggregates of two types of segments and detailed calculations are made of the polarisabilities resulting from the different conformations that occur of both the terephthaloyl and glycol segments. The rotational-isomeric-state (RIS) model for PET chains in melts described previously [9,16–18] is first used to calculate the polarisabilities of the *trans* and *cis* isomers of the terephthaloyl segment and of the different conformations of the glycol segments. The

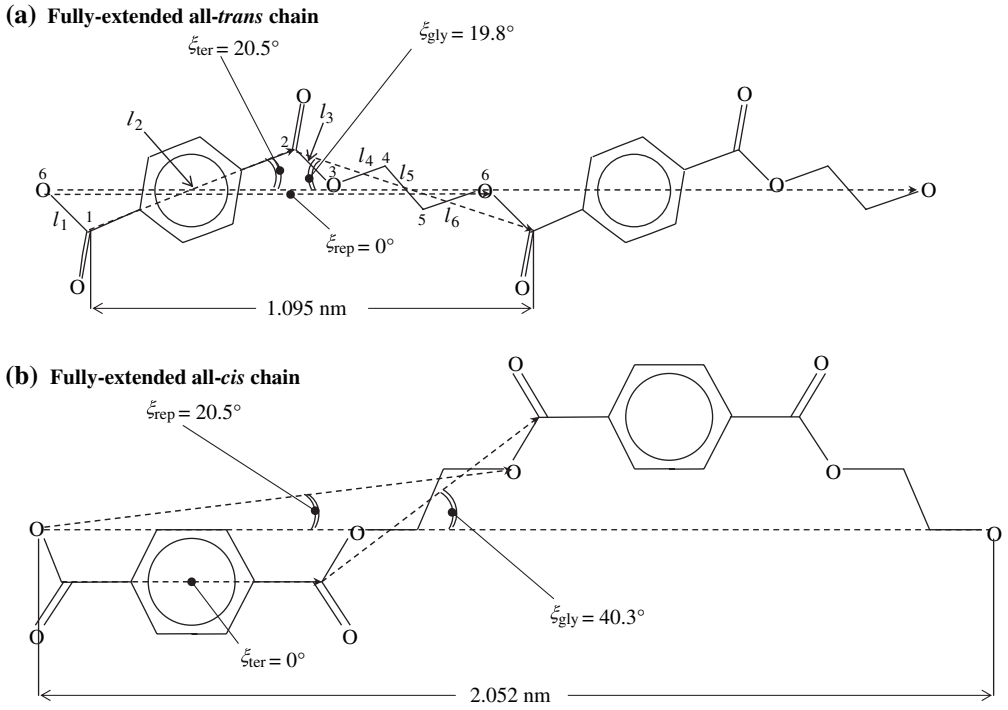

Fig. 1. *Trans* and *cis* PET repeat-unit structures. After Williams and Flory [19]; skeletal atoms are labelled 1–6, and the *i*th skeletal bond connects pairs of atoms with indices i and $i-1$; bond lengths are denoted l_i. The fully-extended length of the *trans* repeat unit is 1.095 nm. The terephthaloyl segment spans from skeletal atoms C1 to C2 and the glycol segment from skeletal atoms C2 to C1. The angles ξ_{ter}, ξ_{gly} and ξ_{rep} are those subtended to the chain end-to-end vector by, respectively, the terephthaloyl segment vector, the glycol segment vector and the repeat-unit segment vector.

latter segments contain five skeletal bonds (see Fig. 1) for which there are 27 possible conformations (see later). The conformational-dependent polarisabilities are then used in the MC network calculations to predict the birefringent properties of drawn PET melts. As part of the modelling approach, a method of pre-averaging the individual glycol polarisabilities is described that greatly reduces the length of the calculation. (See Fig. 6 and related discussion.)

2. Geometry of the PET chain and RIS model

With reference to the *trans*-terephthaloyl and *cis*-terephthaloyl isomers of the six-bond repeat-unit structure shown in Fig. 1, the geometrical parameters (bond lengths, l_i, and valence-angle supplements, θ_i) taken from Williams and Flory [19], are as follows: $l_1 = l_3 = l_{O-C'} = 0.134$ nm (C′ denotes the carbonyl carbon atom), $l_4 = l_6 = l_{O-C} = 0.144$ nm, $l_5 = l_{C-C} = 0.153$ nm, $l_2 = 0.574$ nm (virtual bond), $\theta_1 = \theta_2 = 66°$, $\theta_3 = \theta_6 = 67°$, and $\theta_4 = \theta_5 = 70°$. The terephthaloyl segment vector is defined as lying along the virtual bond, l_2, between the carbonyl carbons; the glycol segment vector is defined as the straight-line joining the carbonyl carbons across the glycol residue; and the repeat-unit vector (indicated by a dashed double-line in Fig. 1(a)) is defined by the straight-line joining successive oxygen atoms labelled 6. It can be seen that a chain of N repeat units has only $N-1$ complete glycol units. The Nth unit is split and is constituted of the first bond in a chain (O6−C1) and the last four bonds in a chain (C2−O6).

Fig. 1(a) shows two repeat units of the fully-extended all-*trans*-terephthaloyl PET chain. In this state, the angle between the terephthaloyl segment and the end-to-end vector, ξ_{ter}, is 20.5°; the angle between the glycol segment and the end-to-end-vector, ξ_{gly}, is 19.8°; and the angle between the repeat-unit vector and the end-to-end vector, ξ_{rep}, is 0°. Fig. 1(b) shows two repeat units of a fully-extended all-*cis*-terephthaloyl PET chain; in this state $\xi_{ter} = 0°$, $\xi_{gly} = 40.3°$ and $\xi_{rep} = 20.5°$.

In RIS models, the statistical weight, $u_{\zeta\eta;i}$ associated with a rotational state η of skeletal bond i is also dependent upon the state ζ at bond $i-1$. The value of $u_{\zeta\eta;i}$ is related to the corresponding rotational energy, $E_{\zeta\eta;i}$, by

$$u_{\zeta\eta;i} = \exp\left(\frac{-E_{\zeta\eta;i}}{RT}\right). \tag{2}$$

The set of interdependent statistical weights pertaining to all rotational states for a given bond pair can be expressed in the form of a statistical weights matrix $U_i = [u_{\zeta\eta;i}]$, with states ζ for bond $i-1$ indexing the rows and states η for bond i indexing the columns. The rotational states are *cis* and *trans* for the terephthaloyl segment and *gauche*$_-$ (g_-), *trans* (t) and *gauche*$_+$ (g_+) for the bonds of the glycol segment. The statistical weight matrices for the six skeletal bonds of the PET repeat unit (see Fig. 1) are listed in the following equations [16,19]:

$$i \neq 2,3;\ U_i = \begin{bmatrix} & g_- & t & g_+ \\ g_- & & & \\ t & & & \\ g_+ & & & \end{bmatrix};\ U_2 = \begin{bmatrix} & cis & trans \\ g_- & & \\ t & & \\ g_+ & & \end{bmatrix};$$

$$U_3 = \begin{bmatrix} & g_- & t & g_+ \\ cis & & & \\ trans & & & \end{bmatrix}$$

$$U_1 = \begin{bmatrix} 0 & 1 & 0 \\ 0 & 1 & 0 \\ 0 & 1 & 0 \end{bmatrix} \tag{3}$$

$$U_2 = \begin{bmatrix} 0 & 0 \\ 1 & 1 \\ 0 & 0 \end{bmatrix} \tag{4}$$

$$U_3 = \begin{bmatrix} 0 & 1 & 0 \\ 0 & 1 & 0 \end{bmatrix} \tag{5}$$

$$U_4 = \begin{bmatrix} 0 & 0 & 0 \\ \sigma_4 & 1 & \sigma_4 \\ 0 & 0 & 0 \end{bmatrix} \tag{6}$$

$$U_5 = \begin{bmatrix} \sigma_5 & 1 & \sigma_5\omega \\ \sigma_5 & 1 & \sigma_5 \\ \sigma_5\omega & 1 & \sigma_5 \end{bmatrix} \tag{7}$$

$$U_6 = \begin{bmatrix} \sigma_6 & 1 & \sigma_6\omega \\ \sigma_6 & 1 & \sigma_6 \\ \sigma_6\omega & 1 & \sigma_6 \end{bmatrix} \tag{8}$$

The model has *gauche* conformational states of bonds 4, 5 and 6 at $\phi_{g\pm} = \pm 120°$. The energies [16,17] associated with the statistical weights σ_4, σ_5, σ_6 and ω are $E_{\sigma_4} = E_{\sigma_6} = 1.75$ kJ mol^{-1}, $E_{\sigma_5} = -4.16$ kJ mol^{-1} and $E_\omega = 5.80$ kJ mol^{-1}.

3. Bond and segmental polarisabilities

Fig. 2 depicts a bond in relation to an external Cartesian coordinate system 0*XYZ*. One end is fixed at the origin. β_1, the component polarisability along the bond, is shown, and β_2 and β_3 (not shown) denote the component polarisabilities perpendicular to the bond. The component bond polarisabilities are assumed to be cylindrically symmetrical, so that $\beta_2 = \beta_3$. Because all values of ϕ are equally probable, one finds that the principle component polarisabilities along the external axes 0*X*, 0*Y* and 0*Z* are given by the equations [20]

$$\beta_x = \beta_1\cos^2\theta + \beta_2\sin^2\theta = \frac{1}{3}(\beta_1 + 2\beta_2) + \frac{2}{3}(\beta_1 - \beta_2)P_2(\cos\theta) \tag{9}$$

$$\beta_y = \beta_z = \frac{1}{3}(\beta_1 + 2\beta_2) - \frac{1}{3}(\beta_1 - \beta_2)P_2(\cos\theta) \tag{10}$$

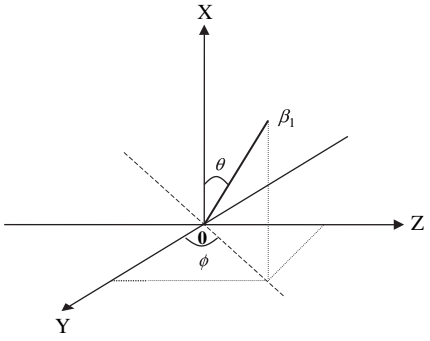

Fig. 2. A bond positioned relative to an external set of Cartesian co-ordinates 0*XYZ*. One end is fixed at the origin; β_1 is the component polarisability along the bond, and β_2 and β_3 (not shown) are the component polarisabilities perpendicular to the bond.

where

$$P_2(\cos\theta) = \frac{1}{2}\left(3\cos^2\theta - 1\right) \tag{11}$$

To treat structural units (segments) composed of several (n_{seg}) bonds, the components of the polarisabilities for the individual bonds are simply added to give

$$\beta_x = \frac{1}{3}\sum_{i=1}^{n_{seg}}\left(\beta_{1,i} + 2\beta_{2,i}\right) + \sum_{i=1}^{n_{seg}}\left(\beta_{1,i} - \beta_{2,i}\right)P_2(\cos\theta_i) \tag{12}$$

$$\beta_y = \frac{1}{3}\sum_{i=1}^{n_{seg}}\left(\beta_{1,i} + 2\beta_{2,i}\right) - \frac{1}{3}\sum_{i=1}^{n_{seg}}\left(\beta_{1,i} - \beta_{2,i}\right)P_2(\cos\theta_i) \tag{13}$$

Finally, if we let 0*X* be the direction of the end-to-end vector of the segment, then θ_i is the angle that bond *i* subtends to that vector.

4. Evaluation of PET segmental polarisabilities

4.1. Terephthaloyl segment

Fig. 3 shows the geometry of the terephthaloyl segment with co-linear rotations giving *trans* and *cis* isomers of equal weight. Because bond polarisabilities are not directional in a negative–positive sense, there is no difference between the segmental polarisabilities of the *cis* and *trans* conformers.

Values of β_x^{ter} and β_y^{ter} for the terephthaloyl segment, calculated using published values of bond polarisabilities due to Bunn and Daubeny [21], Denbigh [22], and LeGrand and Scacchetti [23], are given in Table 1. The bond polarisabilities of Bunn and Daubeny have been conventionally used for PET [4,14,24]. Those of Denbigh, with a larger value of the anisotropy of the polarisabilities of the aliphatic C–C bond and slightly different values of the polarisabilities of the C=O and C–H bonds, have been shown to give quantitative agreement with measured values of $\Delta\tilde{n}$ of PE [12,13]. Sections 1, 2 and 3 of Table 1 show that, because there are proportionately very few aliphatic C–C bonds in PET, there are only small differences that result from the use of the Bunn and Daubeny compared with the Denbigh bond polarisabilities for PET. The LeGrand and Scacchetti bond polarisabilities are the same as those of Denbigh, except for the polarisabilities of the aromatic ring. The origins of the larger parallel polarisability of the aromatic ring are not explained by LeGrand and Scacchetti. The value is not consistent with the valence-optical scheme used to calculate the Denbigh and Bunn and Daubeny polarisabilities.

Because of theoretical reasons [20] and because of the agreement with experiment they give for $\Delta\tilde{n}$ of PE [12,13], we have used Denbigh's bond polarisabilities for discussion

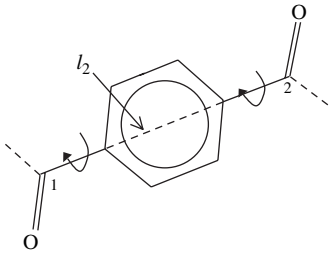

Fig. 3. The terephthaloyl segment (C1 → C2) with bond rotations illustrated. The terminal dashed bonds shown belong to the neighbouring glycol segments.

Table 1
C_6H_4, terephthaloyl, *trans*-glycol and all-*trans* repeat-unit polarisabilities of PET, calculated according to the bond polarisabilities of Bunn and Daubeny [21], Denbigh [22], and LeGrand and Scacchetti [23], together with the refractive indices and related quantities for hypothetical materials having the same density as amorphous PET and constituted of fully-extended all-*trans* PET repeat units

1. C_6H_4 polarisabilities

	Parallel/10^{-25} cm^3	Perpendicular/10^{-25} cm^3
LeGrand and Scacchetti	130.4	79.7
Denbigh	107.7	76.4
Bunn and Daubeny	108.6	82.4

2. Terephthaloyl segment polarisabilities

	Parallel/10^{-25} cm^3 (β_x^{ter})	Perpendicular/10^{-25} cm^3 (β_y^{ter})
LeGrand and Scacchetti	182.8	108.4
Denbigh	160.1	110.1
Bunn and Daubeny	164.2	114.6

3. *trans*-Glycol segment polarisabilities

	Parallel/10^{-25} cm^3 ($\beta_{x,trans}^{gly}$)	Perpendicular/10^{-25} cm^3 ($\beta_{y,trans}^{gly}$)
LeGrand and Scacchetti	79.84	46.68
Denbigh	79.84	46.68
Bunn and Daubeny	73.21	47.30

4. Repeat-unit polarisabilities, refractive indices and maximum birefringence

	$10^{25}p_{\parallel,rep}$/cm^3	$10^{25}p_{\perp,rep}$/cm^3	$\tilde{n}_{\parallel}$	$\tilde{n}_{\perp}$	$\Delta\tilde{n}_{max}$	$\tilde{n}_{iso}$
LeGrand and Scacchetti	250	162	1.829	1.480	0.350	1.596
Denbigh	230	162	1.742	1.480	0.262	1.567
Bunn and Daubeny	228	166	1.735	1.497	0.238	1.576

$p_{\parallel,rep}$ and $p_{\perp,rep}$: repeat-unit polarisabilities parallel and perpendicular, respectively, to the repeat-unit vector. $\tilde{n}_{\parallel}$ and $\tilde{n}_{\perp}$: refractive indices of a material of completely aligned repeat units, parallel and perpendicular, respectively, to the repeat-unit vectors. $\Delta\tilde{n}_{max}$: maximum possible birefringence of PET, $\Delta\tilde{n}_{max} = \tilde{n}_{\parallel} - \tilde{n}_{\perp}$. $\tilde{n}_{iso}$: refractive index of a material of randomly oriented repeat units, $\tilde{n}_{iso} = (\tilde{n}_{\parallel} + 2\tilde{n}_{\perp})/3$.

of the interpretation of experimental results in Paper III [25]. Also, as just stated, the use of Bunn and Daubeny's polarisabilities give values of $\Delta\tilde{n}$ for PET that are only slightly lower than those calculated using Denbigh's polarisabilities. Some comparisons are made in the present paper and in Paper III with the results of using the LeGrand and Scacchetti C_6H_4 polarisabilities. Whilst the calculated values of $\Delta\tilde{n}$ are higher than those calculated using the Denbigh values, it will be seen that the basic molecular interpretation of the behaviour of PET chains on deformation is the same.

4.2. Glycol segment

Fig. 4 shows a glycol segment; the end-to-end vector of the segment is along the line C2 → C1. The evaluation of the polarisability of the segment as a whole requires the summation of the polarisabilities of all of the bonds in the segment and needs to account for the various conformations that can occur. If the bond vectors are expressed in a common co-ordinate system then the segmental polarisabilities β_x^{gly} and β_y^{gly} can be evaluated using Eqs. (12) and (13). The common co-ordinates 0*XYZ* used are defined with respect to the first two bonds. The origin is at C2 and O3 lies along 0*X* having co-ordinates $(x,y,z) = (l_3,0,0)$. Thus, bond vector $\boldsymbol{l}_3 = (l_3,0,0)$. The co-ordinates of C4 are chosen so that $\boldsymbol{l}_4$ has a positive projection on 0*X*. In general, the transformation matrix, $\boldsymbol{T}_i$, transforming bond i into the co-ordinate system of bond $i-1$ is [26]

$$\boldsymbol{T}_i = \begin{pmatrix} \cos\theta_{i-1} & \sin\theta_{i-1} & 0 \\ \sin\theta_{i-1}\cos\phi_{i-1} & -\cos\theta_{i-1}\cos\phi_{i-1} & \sin\phi_{i-1} \\ \sin\theta_{i-1}\sin\phi_{i-1} & -\cos\theta_{i-1}\sin\phi_{i-1} & -\cos\phi_{i-1} \end{pmatrix} \tag{14}$$

Putting $\phi_3 = 0$ as $\boldsymbol{l}_3$ and $\boldsymbol{l}_4$ must be coplanar, bond vector $\boldsymbol{l}_4 = (l_4,0,0)$ can be transformed into the co-ordinate system of bond 3, giving

$$\boldsymbol{l}_4^{\mathrm{I}} = \boldsymbol{T}_4 \cdot \boldsymbol{l}_4 = \begin{pmatrix} l'_{x4} \\ l'_{y4} \\ l'_{z4} \end{pmatrix} = \begin{pmatrix} \cos\theta_3 & \sin\theta_3 & 0 \\ \sin\theta_3 & -\cos\theta_3 & 0 \\ 0 & 0 & -1 \end{pmatrix} \begin{pmatrix} l_4 \\ 0 \\ 0 \end{pmatrix} = \begin{pmatrix} l_4\cos\theta_3 \\ l_4\sin\theta_3 \\ 0 \end{pmatrix}. \tag{15}$$

Fig. 5 shows that the co-ordinates of C5, H41 and H42 depend on the conformational angle ϕ_4 and the valence angles $\widehat{OCC} = \theta_4$, $\widehat{OCH41}$, and $\widehat{OCH42}$. For the model used

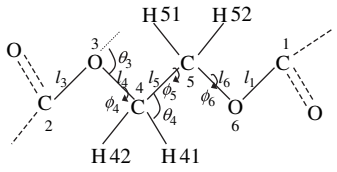

Fig. 4. The glycol segment (C2 → C1) showing bond lengths, valence angles, conformational angles, hydrogen atoms and skeletal-bond rotational angles. The dashed bonds shown belong to the neighbouring terephthaloyl segments.

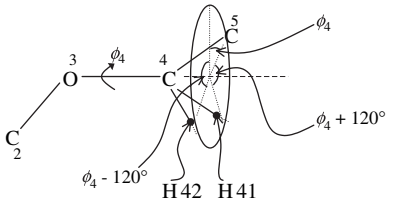

Fig. 5. Defining the positions of C5 and the hydrogen atoms H41 and H42 due to rotation about skeletal bond 4.

[16,17,19,26], all these angles are assumed to be equal to 70°. Also, $\phi_4 = -120°$, 0°, 120° define the g_-, t, and g_+ states of the C2—O3—C4—C5 sequence. The co-ordinates of C5 are $(l_5,0,0)$ in its local co-ordinate system (0*X* along l_5) and they can be transformed into the co-ordinate system of bond 4 to give $\boldsymbol{l}'_5 = (l'_{x5}, l'_{y5}, l'_{z5})$, with

$$\begin{pmatrix} l'_{x5} \\ l'_{y5} \\ l'_{z5} \end{pmatrix} = \begin{pmatrix} \cos\theta_4 & \sin\theta_4 & 0 \\ \sin\theta_4\cos\phi_4 & -\cos\theta_4\cos\phi_4 & \sin\phi_4 \\ \sin\theta_4\sin\phi_4 & -\cos\theta_4\sin\phi_4 & -\cos\phi_4 \end{pmatrix} \begin{pmatrix} l_5 \\ 0 \\ 0 \end{pmatrix} \tag{16}$$

The bonds C4−H41 and C4−H42 are treated similarly to bond l_5 but $\phi_4 \Rightarrow \phi_4 + 120°$ for C4−H41 and $\phi_4 - 120°$ for C4−H42. Thus,

$$\boldsymbol{l}_5^{\mathrm{I}} = \boldsymbol{T}_5 \cdot \boldsymbol{l}_5, \tag{17}$$

$$\boldsymbol{l}_{\mathrm{H41}}^{\mathrm{I}} = \boldsymbol{T}_{\mathrm{H41}} \cdot \boldsymbol{l}_{\mathrm{H41}} \tag{18}$$

$$\text{and } \boldsymbol{l}_{\mathrm{H42}}^{\mathrm{I}} = \boldsymbol{T}_{\mathrm{H42}} \cdot \boldsymbol{l}_{\mathrm{H42}}, \tag{19}$$

where $\boldsymbol{l}_i = (l_i,0,0)$. For $\boldsymbol{T}_5$, $\theta = \theta_4$, $\phi = \phi_4$; for $\boldsymbol{T}_{\mathrm{H41}}$, $\theta = \theta_4$, $\phi = \phi_4 + 120°$; and, for $\boldsymbol{T}_{\mathrm{H42}}$, $\theta = \theta_4$, $\phi = \phi_4 - 120°$.

The bond vectors $\boldsymbol{l}_5$, $\boldsymbol{l}_{\mathrm{H41}}$, $\boldsymbol{l}_{\mathrm{H42}}$ need to be further transposed by rotation using $\boldsymbol{T}_4$, to give, in terms of the co-ordinate system of bond 3

$$\boldsymbol{l}_5^{\mathrm{II}} = \boldsymbol{T}_4 \cdot \boldsymbol{T}_5 \cdot \boldsymbol{l}_5, \tag{20}$$

$$\boldsymbol{l}_{\mathrm{H41}}^{\mathrm{II}} = \boldsymbol{T}_4 \cdot \boldsymbol{T}_{\mathrm{H41}} \cdot \boldsymbol{l}_{\mathrm{H41}} \tag{21}$$

and

$$\boldsymbol{l}_{\mathrm{H42}}^{\mathrm{II}} = \boldsymbol{T}_4 \cdot \boldsymbol{T}_{\mathrm{H42}} \cdot \boldsymbol{l}_{\mathrm{H42}}. \tag{22}$$

Continuing this process over the remaining bonds in the glycol unit gives, for the bond vectors in the co-ordinate system of bond 3,

$$\boldsymbol{l}_6^{\mathrm{III}} = \boldsymbol{T}_4 \cdot \boldsymbol{T}_5 \cdot \boldsymbol{T}_6 \cdot \boldsymbol{l}_6, \tag{23}$$

$$\boldsymbol{l}_{\mathrm{H51}}^{\mathrm{III}} = \boldsymbol{T}_4 \cdot \boldsymbol{T}_5 \cdot \boldsymbol{T}_{\mathrm{H51}} \cdot \boldsymbol{l}_{\mathrm{H51}}, \tag{24}$$

$$\boldsymbol{l}_{\mathrm{H52}}^{\mathrm{III}} = \boldsymbol{T}_4 \cdot \boldsymbol{T}_5 \cdot \boldsymbol{T}_{\mathrm{H52}} \cdot \boldsymbol{l}_{\mathrm{H52}} \tag{25}$$

and

$$\boldsymbol{l}_1^{\mathrm{IV}} = \boldsymbol{T}_4 \cdot \boldsymbol{T}_5 \cdot \boldsymbol{T}_6 \cdot \boldsymbol{T}_1 \cdot \boldsymbol{l}_1, \tag{26}$$

where the bonds C5−H51 and C5−H52 are treated similarly to bond l_6 but $\phi_5 \Rightarrow \phi_5 + 120^\circ$ for C5−H51 and $\phi_5 \Rightarrow \phi_5 - 120^\circ$ for C5−H52.

The end-to-end vector of the glycol segment in the co-ordinate system of bond 3 is

$$\boldsymbol{r} = \begin{pmatrix} r_x \\ r_y \\ r_z \end{pmatrix} = \boldsymbol{l}_3 + \boldsymbol{l}_4^{\mathrm{I}} + \boldsymbol{l}_5^{\mathrm{II}} + \boldsymbol{l}_6^{\mathrm{III}} + \boldsymbol{l}_1^{\mathrm{IV}}. \tag{27}$$

The angle, θ, between $\boldsymbol{r}$ and a bond vector $\boldsymbol{l}_i$ is

$$\cos\theta_i = \frac{\boldsymbol{l}_i \cdot \boldsymbol{r}}{l_i r} \tag{28}$$

$\boldsymbol{l}_i$ is, of course, expressed in the same co-ordinate system as $\boldsymbol{r}$ and can be equal to $\boldsymbol{l}_3, \boldsymbol{l}_4^{\mathrm{I}}, \boldsymbol{l}_5^{\mathrm{II}}, \ldots, \boldsymbol{l}_{\mathrm{H52}}^{\mathrm{III}}$ or $\boldsymbol{l}_1^{\mathrm{IV}}$.

The glycol segmental polarisabilities along and perpendicular to the segment (end-to-end) vector, β_x^{gly} and β_y^{gly}, for the segment in a *given* conformation can now be found using Eqs. (12) and (13). Summing over the 9 bonds in a glycol segment gives:

$$\beta_x^{\mathrm{gly}} = \frac{1}{3}\sum_{k=1}^{9}\left(\beta_{1,k} + 2\beta_{2,k}\right) + \frac{2}{3}\sum_{k=1}^{9}\left(\beta_{1,k} - \beta_{2,k}\right)P_2(\cos\theta_k) \tag{29}$$

$$\beta_y^{\mathrm{gly}} = \frac{1}{3}\sum_{k=1}^{9}\left(\beta_{1,k} + 2\beta_{2,k}\right) - \frac{1}{3}\sum_{k=1}^{9}\left(\beta_{1,k} - \beta_{2,k}\right)P_2(\cos\theta_k) \tag{30}$$

There are 3^3 isomers of the glycol segment, corresponding to ϕ_4, ϕ_5, ϕ_6, and each having 3 values (ϕ_{g-}, ϕ_t, ϕ_{g+}) = (−120°, 0°, 120°). Illustrative calculated values of β_x^{gly} and β_y^{gly} for the 27 isomers using the Denbigh (or LeGrand and Scacchetti) bond polarisabilities are given in Table 2. (Both sets of authors give the same polarisabilities for the bonds of the glycol unit.) The statistical weight of a segmental conformation is denoted $\tau_{4,5,6}$ in Table 2. For example, from Eqs. (6)−(8), $\tau_{4,5,6} = \sigma_4 \cdot \sigma_5 \omega \cdot \sigma_6$ for ϕ_4, ϕ_5 and ϕ_6 having the particular rotational states of g_-, g_+ and g_+. The probability of a conformation is $\tau_{4,5,6}/Z$, where Z is the segmental partition function [26].

$$Z = \boldsymbol{J}^* \left[\prod_{i=4}^{6} U_i\right] \boldsymbol{J} \tag{31}$$

with

$$\boldsymbol{J}^* = [1 \quad 0 \quad 0]; \; \boldsymbol{J} = \begin{bmatrix} 1 \\ 1 \\ 1 \end{bmatrix} \tag{32}$$

The probabilities multiplied by β_x^{gly} and β_y^{gly} give the contributions of individual glycol conformations to the average segmental polarisability. These contributions are summarised in the final two columns of Table 2. Summing over these entries gives the average values $\langle\beta_x^{\mathrm{gly}}\rangle = 68.06 \times 10^{-25}$ cm^3 and

Table 2
Glycol segmental polarisabilities, β_x^{gly} and β_y^{gly}, based on Denbigh [22] (or LeGrand and Scacchetti [23]) bond polarisabilities for the 27 possible conformations of the glycol segment in PET, their probabilities ($\tau_{4,5,6}/Z$) at 523 K and contributions to the average segmental polarisabilities $\langle\beta_x^{\mathrm{gly}}\rangle$ and $\langle\beta_y^{\mathrm{gly}}\rangle$

ϕ_4	ϕ_5	ϕ_6	$10^{25}\,\beta_x$/cm^3	$10^{25}\,\beta_y$/cm^3	$\tau_{4,5,6}/Z$	$10^{25}\,\beta_x\,(\tau_{4,5,6}/Z)$/cm^3	$10^{25}\,\beta_y\,(\tau_{4,5,6}/Z)$/cm^3
t	t	t	79.84	46.68	0.038	3.04	1.77
t	g_+	t	77.81	47.69	0.157	12.21	7.48
t	g_-	t	77.81	47.69	0.157	12.21	7.48
g_+	t	g_-	67.36	52.92	0.012	0.78	0.61
g_-	t	g_+	67.36	52.92	0.012	0.78	0.61
t	t	g_+	68.24	52.48	0.021	1.43	1.10
t	t	g_-	68.24	52.48	0.021	1.43	1.10
g_+	t	t	67.74	52.73	0.021	1.42	1.11
g_-	t	t	67.74	52.73	0.021	1.42	1.11
g_+	t	g_+	63.37	54.92	0.012	0.73	0.64
g_-	t	g_-	63.37	54.92	0.012	0.73	0.64
g_+	g_+	g_+	60.70	56.25	0.048	2.90	2.69
g_-	g_-	g_-	60.70	56.25	0.048	2.90	2.69
t	g_+	g_-	65.19	54.00	0.012	0.78	0.65
t	g_-	g_+	65.19	54.00	0.012	0.78	0.65
t	g_+	g_+	62.34	55.43	0.087	5.40	4.80
t	g_-	g_-	62.34	55.43	0.087	5.40	4.80
g_+	g_-	t	64.36	54.42	0.012	0.77	0.65
g_-	g_+	t	64.36	54.42	0.012	0.77	0.65
g_+	g_+	t	61.59	55.81	0.087	5.33	4.83
g_-	g_-	t	61.59	55.81	0.087	5.33	4.83
g_-	g_+	g_+	53.42	59.89	0.007	0.35	0.40
g_+	g_-	g_-	53.42	59.89	0.007	0.35	0.40
g_+	g_+	g_-	53.24	59.98	0.007	0.35	0.40
g_-	g_-	g_+	53.24	59.98	0.007	0.35	0.40
g_+	g_-	g_+	56.92	58.14	0.001	0.05	0.05
g_-	g_+	g_-	56.92	58.14	0.001	0.05	0.05
					1.000	$\langle\beta_x^{\mathrm{gly}}\rangle = 68.06$	$\langle\beta_y^{\mathrm{gly}}\rangle = 52.57$

$\langle\beta_y^{gly}\rangle = 52.57 \times 10^{-25}$ cm^3. The difference between these two values is much less than that given by the all-*trans* conformations, for which Table 1 and the first row in Table 2 give $\beta_{x,trans}^{gly} = 79.84 \times 10^{-25}$ cm^3 and $\beta_{y,trans}^{gly} = 46.68 \times 10^{-25}$ cm^3.

We have tested two approaches for calculating the average glycol segmental polarisability in a PET chain of a given number of repeat units. First, the polarisabilities for the individual glycol conformations (β_x^{gly} and β_y^{gly}) are summed over all the segments in a network and the average evaluated. Second, the average values ($\langle\beta_x^{gly}\rangle$ and $\langle\beta_y^{gly}\rangle$) are used for each glycol segment. The latter approach results in a much simpler and shorter calculation and is found (see later) to introduce negligible numerical errors.

5. MC simulations of the orientation of bonds, segments and network chains

In order to determine the contribution of the polarisability of a segment to the polarisability of a network sample, it is necessary to express each segment vector in the external laboratory co-ordinates of the network in which the (uniaxial) strain is expressed. As illustrated in Fig. 5 of Paper I, this resolution of vectors is achieved by evaluating the angle (ξ) that the segment vector subtends to the end-to-end vector of the chain ($\boldsymbol{r}$) and the angle (ψ) that $\boldsymbol{r}$ subtends to the uniaxial strain [12,13]. It is assumed that all positions on the cone defined by ξ are equally probable. The Legendre addition theorem can then be used [27] to define the (average) orientation function $P_2(\cos\zeta)$ of the segment relative to the strain direction with

$$P_2(\cos\zeta) = P_2(\cos\xi)\cdot P_2(\cos\psi) \tag{33}$$

ζ is the effective angle between the segment and the strain direction, consistent with the value of $P_2(\cos\zeta)$ given by Eq. (33). Further, it should be noted that, although Fig. 5 of Paper I refers to segment vectors, it can apply equally well to individual bond vectors. Thus, we may use ξ and ζ as angles describing orientations of any vector associated with a chain once its co-ordinates are expressed in the common Cartesian co-ordinate system for the chain.

In the MC method of generating chains in networks [10,11], samples of chains distributed according to $W(r)$, the radial distribution function, are generated. Sample sizes of about 3×10^6 chains are used to match the values of $\langle r^2\rangle$ with the exact values calculated using matrix algebra [26]. The Cartesian co-ordinate system for bond vectors is defined by the first two skeletal bonds in a chain, l_1 and l_2 in Fig. 1, and the transformation matrices, $\boldsymbol{T}_i$, for all the bonds within segments (see Section 4.2) used to transform atom co-ordinates from their local co-ordinate systems to those expressed in the common co-ordinate system for the whole chain.

A network is constructed by growing a population of chains with end-to-end distances distributed according to $W(r)$ randomly oriented in external space. In the MC network deformation algorithm, a sample of $N \approx 5 \times 10^6$ individual chains is chosen from the population and subjected to a range of uniaxial macroscopic deformation ratios, λ, in a fixed external direction. The deformation is affine up to $r = r^*_{max}$, the effective conformationally fully-extended end-to-end distance of the polymer chain. The significance of r^*_{max} has been discussed previously [10,11]. The MC sample has $W(r > r^*_{max}) = 0$ and no conformations occur in this range of r. Thus, for $r > r^*_{max}$ a chain vector merely rotates to align, eventually with the deformation axis. This latter deformation is equivalent to the pseudo-affine deformation scheme [7].

For a chain that is grown, the angle ξ subtended to the end-to-end vector ($\boldsymbol{r}$) is known for each of its bonds. In addition, the skeletal bonds can be grouped into segments and the angles ξ_{seg}, between the segment vectors and $\boldsymbol{r}$, are also known. Further, at a given λ, the angle ψ between $\boldsymbol{r}$ and the strain axis is known.

6. Birefringence and segmental polarisabilities

For bulk polymer, the components of the refractive indices parallel ($\tilde{n}_\parallel$) and perpendicular ($\tilde{n}_\perp$) to the direction of the applied strain can be expressed (through the Lorentz–Lorenz equation) in terms of the molar masses (M_{rep}) and the average parallel and perpendicular components of the polarisabilities ($\langle p_{\parallel,rep}\rangle$ and $\langle p_{\perp,rep}\rangle$) of the repeat units.

$$\tilde{n}_\parallel = \left(\frac{3 + 8\pi\rho\frac{N_{Av}}{M_{rep}}\langle p_{\parallel,rep}\rangle}{3 - 4\pi\rho\frac{N_{Av}}{M_{rep}}\langle p_{\parallel,rep}\rangle}\right)^{1/2} \tag{34}$$

and

$$\tilde{n}_\perp = \left(\frac{3 + 8\pi\rho\frac{N_{Av}}{M_{rep}}\langle p_{\perp,rep}\rangle}{3 - 4\pi\rho\frac{N_{Av}}{M_{rep}}\langle p_{\perp,rep}\rangle}\right)^{1/2}, \tag{35}$$

where ρ is the density of the sample. The birefringence is

$$\Delta\tilde{n} = \tilde{n}_\parallel - \tilde{n}_\perp. \tag{36}$$

The predicted values of $\langle p_{\parallel,rep}\rangle$ and $\langle p_{\perp,rep}\rangle$ are the average values over the MC samples of repeat units. For randomly oriented repeat units, $\langle p_{\parallel,rep}\rangle = \langle p_{\perp,rep}\rangle$ and $\Delta\tilde{n} = 0$.

For small values of $\Delta\tilde{n}$ (i.e. $\Delta\tilde{n} \ll \tilde{n}_\parallel, \tilde{n}_\perp$), Eq. (36) can be written as [20,28]

$$\Delta\tilde{n} = \frac{2}{9}\pi\rho\frac{N_{Av}}{M_{rep}}\frac{\left(\tilde{n}_o^2 + 2\right)^2}{\tilde{n}_o}\left(\langle p_{\parallel,rep}\rangle - \langle p_{\perp,rep}\rangle\right). \tag{37}$$

$\tilde{n}_o$ is equal to the isotropic value of the refractive index at zero strain. Also, Eq. (37) assumes that

$$\tilde{n}_o = \left(\tilde{n}_\parallel + \tilde{n}_\perp\right)/2 \tag{38}$$

and that $\tilde{n}_o \approx \tilde{n}_\parallel \approx \tilde{n}_\perp$.

The expressions for $\langle p_{\parallel,rep}\rangle$ and $\langle p_{\perp,rep}\rangle$ can be written in terms of the terephthaloyl and glycol segmental polarisabilities perpendicular and parallel to the strain direction, giving

$$\langle p_{\parallel,rep}\rangle = \langle p_{\parallel,ter}\rangle + \langle p_{\parallel,gly}\rangle \tag{39}$$

$$\langle p_{\perp,\mathrm{rep}}\rangle = \langle p_{\perp,\mathrm{ter}}\rangle + \langle p_{\perp,\mathrm{gly}}\rangle \tag{40}$$

where, because β_x^{ter} and β_y^{ter} are constants, independent of conformational angles and β_x^{gly} and β_y^{gly} are not independent of $P_2(\cos\zeta_{\mathrm{gly}})$ (compare Eqs. (12) and (13))

$$\langle p_{\parallel,\mathrm{ter}}\rangle = \frac{1}{3}\left(\beta_x^{\mathrm{ter}} + 2\beta_y^{\mathrm{ter}}\right) + \frac{2}{3}\left(\beta_x^{\mathrm{ter}} - \beta_y^{\mathrm{ter}}\right)\langle P_2(\cos\zeta_{\mathrm{ter}})\rangle, \tag{41}$$

$$\langle p_{\perp,\mathrm{ter}}\rangle = \frac{1}{3}\left(\beta_x^{\mathrm{ter}} + 2\beta_y^{\mathrm{ter}}\right) - \frac{1}{3}\left(\beta_x^{\mathrm{ter}} - \beta_y^{\mathrm{ter}}\right)\langle P_2(\cos\zeta_{\mathrm{ter}})\rangle, \tag{42}$$

$$\langle p_{\parallel,\mathrm{gly}}\rangle = \frac{1}{3}\left\langle\left(\beta_x^{\mathrm{gly}} + 2\beta_y^{\mathrm{gly}}\right)\right\rangle + \frac{2}{3}\left\langle\left(\beta_x^{\mathrm{gly}} - \beta_y^{\mathrm{gly}}\right)P_2(\cos\zeta_{\mathrm{gly}})\right\rangle \tag{43}$$

and

$$\langle p_{\perp,\mathrm{gly}}\rangle = \frac{1}{3}\left\langle\left(\beta_x^{\mathrm{gly}} + 2\beta_y^{\mathrm{gly}}\right)\right\rangle - \frac{1}{3}\left\langle\left(\beta_x^{\mathrm{gly}} - \beta_y^{\mathrm{gly}}\right)P_2(\cos\zeta_{\mathrm{gly}})\right\rangle. \tag{44}$$

Also, from Eq. (33)

$$\langle P_2(\cos\zeta_{\mathrm{ter}})\rangle = \langle P_2(\cos\xi_{\mathrm{ter}})\cdot P_2(\cos\psi)\rangle. \tag{45}$$

$\langle P_2(\cos\zeta_{\mathrm{ter}})\rangle$ is averaged over all terephthaloyl segments in the MC sample used. If there are N chains in the sample and each chain contains n repeat units then

$$\langle P_2(\cos\zeta_{\mathrm{ter}})\rangle = \frac{1}{Nn}\sum_{i=1}^{N}\sum_{j=1}^{n}P_2(\cos\zeta_{\mathrm{ter},ij}) = \frac{1}{Nn}\sum_{i=1}^{N}\sum_{j=1}^{n}P_2(\cos\xi_{\mathrm{ter},ij})\cdot P_2(\cos\psi_i). \tag{46}$$

No weighting factor is required as the Metropolis sampling used means that chains are generated in proportion to their statistical weights.

The expressions for $\langle p_{\parallel,\mathrm{gly}}\rangle$ and $\langle p_{\perp,\mathrm{gly}}\rangle$ depend on the conformations of the individual segments as well as their orientation functions. The averages $\langle(\beta_x^{\mathrm{gly}} + 2\beta_y^{\mathrm{gly}})\rangle$ and $\langle(\beta_x^{\mathrm{gly}} - \beta_y^{\mathrm{gly}})P_2(\cos\zeta_{\mathrm{gly}})\rangle$ are again over all the segments in the MC sample, so for N chains each containing n repeat units,

$$\left\langle\left(\beta_x^{\mathrm{gly}} + 2\beta_y^{\mathrm{gly}}\right)\right\rangle = \langle\beta_x^{\mathrm{gly}}\rangle + 2\left\langle\beta_y^{\mathrm{gly}}\right\rangle = \frac{1}{Nn}\sum_{i=1}^{N}\sum_{j=1}^{n}\beta_{x,ij}^{\mathrm{gly}} + \frac{2}{Nn}\sum_{i=1}^{N}\sum_{j=1}^{n}\beta_{y,ij}^{\mathrm{gly}} \tag{47}$$

$$\left\langle\left(\beta_x^{\mathrm{gly}} - \beta_y^{\mathrm{gly}}\right)P_2(\cos\zeta_{\mathrm{gly}})\right\rangle = \frac{1}{Nn}\sum_{i=1}^{N}\sum_{j=1}^{n}\left(\beta_{x,ij}^{\mathrm{gly}} - \beta_{y,ij}^{\mathrm{gly}}\right) \times P_2(\cos\zeta_{\mathrm{gly},ij}) \tag{48}$$

As mentioned previously, the expressions and the calculations can be greatly simplified if each glycol segment is assumed to contribute its average polarisabilities, as calculated in Table 2. In that case,

$$\langle p_{\parallel,\mathrm{gly}}\rangle = \frac{1}{3}\left(\langle\beta_x^{\mathrm{gly}}\rangle + 2\langle\beta_y^{\mathrm{gly}}\rangle\right) + \frac{2}{3}\left(\langle\beta_x^{\mathrm{gly}}\rangle - \langle\beta_y^{\mathrm{gly}}\rangle\right)\langle P_2(\cos\zeta_{\mathrm{gly}})\rangle \tag{49}$$

and

$$\langle p_{\perp,\mathrm{gly}}\rangle = \frac{1}{3}\left(\langle\beta_x^{\mathrm{gly}}\rangle + 2\langle\beta_y^{\mathrm{gly}}\rangle\right) - \frac{1}{3}\left(\langle\beta_x^{\mathrm{gly}}\rangle - \langle\beta_y^{\mathrm{gly}}\rangle\right)\langle P_2(\cos\zeta_{\mathrm{gly}})\rangle, \tag{50}$$

where

$$\langle P_2(\cos\zeta_{\mathrm{gly}})\rangle = \frac{1}{Nn}\sum_{i=1}^{N}\sum_{j=1}^{n}P_2(\cos\zeta_{\mathrm{gly},ij}) = \frac{1}{Nn}\sum_{i=1}^{N}\sum_{j=1}^{n}P_2(\cos\xi_{\mathrm{gly},ij})\cdot P_2(\cos\psi_i) = \langle P_2(\cos\xi_{\mathrm{gly}})\cdot P_2(\cos\psi)\rangle. \tag{51}$$

Note that $\cos\zeta_{\mathrm{gly},ij} \neq \cos\zeta_{\mathrm{ter},ij}$ as Fig. 1 shows that the terephthaloyl and glycol segments are not co-linear.

7. Segmental orientation and polarisability as functions of chain extension

It is useful to evaluate the segmental polarisabilities with respect to the direction of the chain end-to-end vector as a function of chain extension $r/r_{\max}$, where $r_{\max}$ is the end-to-end distance of the geometrically fully-extended all-*trans* chain. The evaluation is equivalent to putting $P_2(\cos\psi) = 1$ in Eqs. (41–51) so that $P_2(\cos\zeta_{\mathrm{ter}}) = P_2(\cos\xi_{\mathrm{ter}})$ and $P_2(\cos\zeta_{\mathrm{gly}}) = P_2(\cos\xi_{\mathrm{gly}})$. The average polarisabilities evaluated can be denoted $\langle p_{\parallel}(\xi_{\mathrm{ter}})\rangle$, $\langle p_{\perp}(\xi_{\mathrm{ter}})\rangle$, $\langle p_{\parallel}(\xi_{\mathrm{gly}})\rangle$, $\langle p_{\perp}(\xi_{\mathrm{gly}})\rangle$, $\langle p_{\parallel}(\xi_{\mathrm{rep}})\rangle$ and $\langle p_{\perp}(\xi_{\mathrm{rep}})\rangle$ to distinguish them from the polarisabilities with respect to the strain direction.

Fig. 6 shows $\langle p_{\parallel}(\xi_{\mathrm{gly}})\rangle$ and $\langle p_{\perp}(\xi_{\mathrm{gly}})\rangle$ plotted versus $r/r_{\max}$ for a PET chain of 120 bonds and evaluated using the Bunn and Daubeny bond polarisabilities and the two different methods of calculation described at the end of Section 4.2. First, the individual values of β_x^{gly} and β_y^{gly} sampled for each glycol segment in the MC simulation have been used according to Eqs. (43) and (44). Second, the pre-averaged values $\langle\beta_x^{\mathrm{gly}}\rangle$ and $\langle\beta_y^{\mathrm{gly}}\rangle$ have been used, with $\langle p_{\parallel}(\xi_{\mathrm{gly}})\rangle$ and $\langle p_{\perp}(\xi_{\mathrm{gly}})\rangle$ calculated using Eqs. (49) and (50). The maximum errors that arise by assuming all of the glycol segments behave like an average glycol segment occur at the largest value of $r/r_{\max}$ sampled, namely, 1.5% for $\langle p_{\parallel}(\xi_{\mathrm{gly}})\rangle$ and 0.9% for $\langle p_{\perp}(\xi_{\mathrm{gly}})\rangle$ at $r/r_{\max} = 0.49$. The apparent small maximum in $\langle p_{\parallel}(\xi_{\mathrm{gly}})\rangle$ and the small minimum in $\langle p_{\perp}(\xi_{\mathrm{gly}})\rangle$ calculated using the individual β_x^{gly} and β_y^{gly} sampled are not significant. They are due to the small number of chains sampled at the larger values of $r/r_{\max}$. For the intermediate values of $r/r_{\max}$, it can be seen that the use of $\langle\beta_x^{\mathrm{gly}}\rangle$ and $\langle\beta_y^{\mathrm{gly}}\rangle$ introduces small, systematic errors that are difficult to explain without investigating the

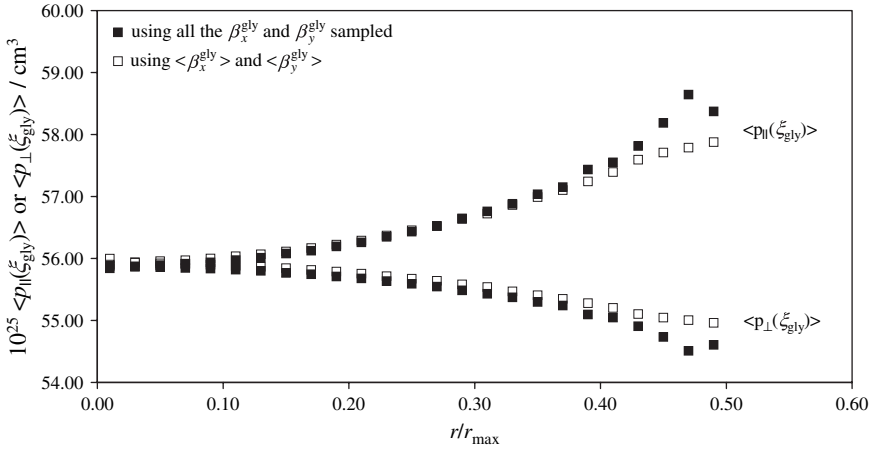

Fig. 6. $\langle p_{\parallel}(\xi_{gly})\rangle$ and $\langle p_{\perp}(\xi_{gly})\rangle$ for the glycol segments versus r/r_{max} for a PET chain of 120 bonds (20 repeat units) at 523 K, based on Bunn and Daubeny bond polarisabilities [21], and using the individual values of β_x^{gly} and β_y^{gly} sampled and the weighted averages $\langle\beta_x^{gly}\rangle$ and $\langle\beta_y^{gly}\rangle$.

contributions of the various glycol conformers to the values of $\langle p_{\parallel}(\xi_{gly})\rangle$ and $\langle p_{\perp}(\xi_{gly})\rangle$ at the various values of r/r_{max}.

Fig. 7 shows $\langle p_{\parallel}(\xi_{rep})\rangle$ and $\langle p_{\perp}(\xi_{rep})\rangle$ plotted versus r/r_{max}, for the same chain and bond polarisabilities as those used in Fig. 6 and evaluated using Eqs. (39) and (40). It can be seen that the results calculated using $\langle\beta_x^{gly}\rangle$ and $\langle\beta_y^{gly}\rangle$ (open symbols) are in agreement, to within 0.25% at the highest values of r/r_{max} sampled, with those calculated using β_x^{gly} and β_y^{gly} for each conformation sampled, averaged over the MC sample. This agreement means it is possible to remove a cumbersome stage from the MC calculation of network polarisabilities by pre-averaging the polarisabilities of the glycol segments rather than calculating them for every conformation sampled. This conclusion also holds if the Denbigh or LeGrand and Scacchetti bond polarisabilities are used.

The terephthaloyl and glycol contributions to the repeat-unit polarisabilities in Fig. 7 are shown in Fig. 8. As expected, the polarisability of the terephthaloyl segment is dominant, but that of the glycol segment is not negligible. The larger anisotropies of the terephthaloyl and repeat unit polarisabilities resulting from using the LeGrand and Scacchetti bond polarisabilities are apparent.

It should be mentioned that, in all of the calculations described, the vector representing the incomplete terminal glycol segment, discussed earlier in Section 2, in relation to Fig. 1, has been taken to span only atoms C2 to O6. Also, to calculate its polarisability $\phi_6 = 0^\circ$ was assumed. The errors introduced by these approximations were calculated by using a computationally more intensive method (taking 3–4 times longer) of calculating $\langle p_{\parallel}(\xi_{rep})\rangle$ and $\langle p_{\perp}(\xi_{rep})\rangle$. The chains were not divided into segments and, for each chain, the contributions of the individual bond polarisabilities to $\langle p_{\parallel}(\xi_{rep})\rangle$ and $\langle p_{\perp}(\xi_{rep})\rangle$ were summed directly. In this way, it was shown that the approximation introduced negligible errors ($\ll$0.001%) into the values of $\langle p_{\parallel}(\xi_{rep})\rangle$ and $\langle p_{\perp}(\xi_{rep})\rangle$.

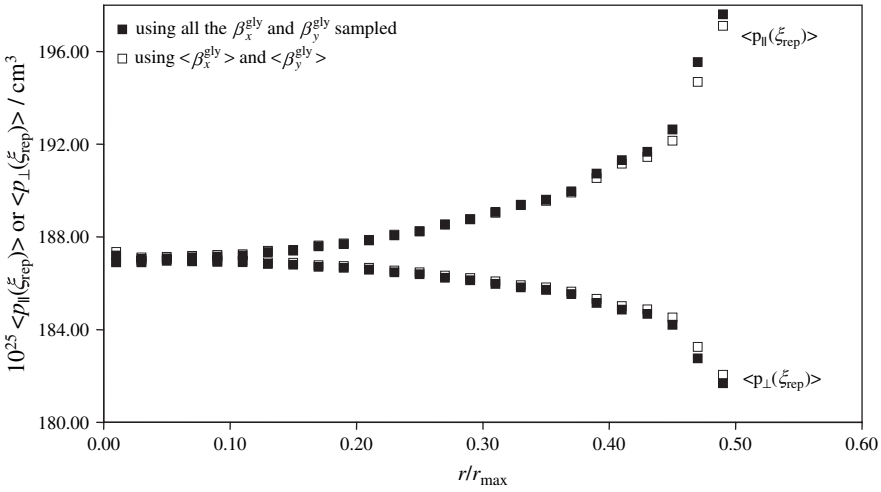

Fig. 7. $\langle p_{\parallel}(\xi_{rep})\rangle$ and $\langle p_{\perp}(\xi_{rep})\rangle$ versus r/r_{max} for a PET chain of 120 bonds (20 repeat units) at 523 K, based on Bunn and Daubeny bond polarisabilities [21], and using the individual values of β_x^{gly} and β_y^{gly} sampled and the weighted averages $\langle\beta_x^{gly}\rangle$ and $\langle\beta_y^{gly}\rangle$.

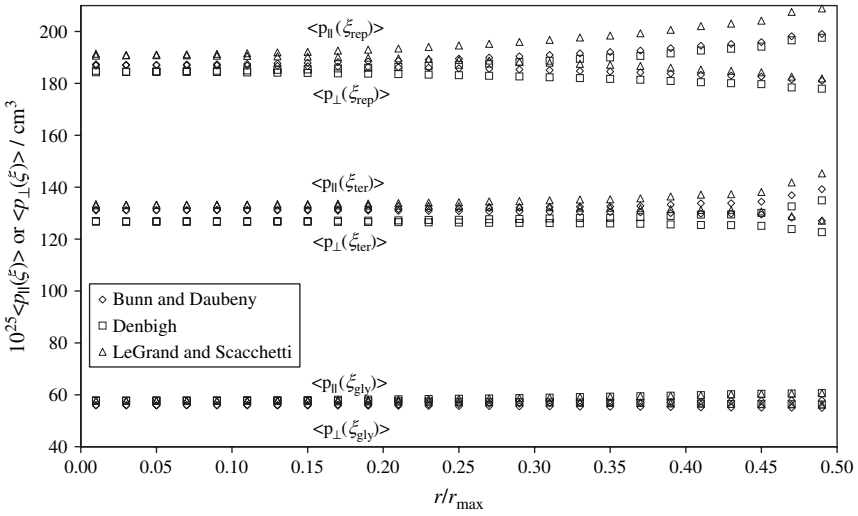

Fig. 8. $\langle p_{\parallel}(\xi)\rangle$ and $\langle p_{\perp}(\xi)\rangle$, for the glycol segments, terephthaloyl segments and repeat units, versus r/r_{max} for a PET chain of 120 bonds (20 repeat units) at 523 K, calculated using the weighted averages $\langle\beta_x^{gly}\rangle$ and $\langle\beta_y^{gly}\rangle$. Values calculated using Bunn and Daubeny [21], Denbigh [22], and LeGrand and Scacchetti [23] bond polarisabilities.

8. Segmental and chain polarisabilities and birefringence in PET networks

Fig. 9 shows the MC values of $\langle p_{\parallel,rep}\rangle$ and $\langle p_{\perp,rep}\rangle$, calculated using Eqs. (39)–(42), (49) and (50), versus deformation ratio, λ, for PET chains of 60, 84, 108 and 150 bonds. The Denbigh bond polarisabilities [22] have been used. Curves of a similar shape are obtained if the Bunn and Daubeny [21] or the LeGrand and Scacchetti bond polarisabilities are used. The values of $\langle p_{\parallel,rep}\rangle$ and $\langle p_{\perp,rep}\rangle$ resulting from the use of the Bunn and Daubeny bond polarisabilities are on an average less than 1% lower than those shown in Fig. 9, whilst the values of $\langle p_{\parallel,rep}\rangle$ resulting from use of the LeGrand and Scacchetti polarisabilities are some 2% higher and only slightly different in $\langle p_{\perp,rep}\rangle$. Such differences are consistent with the values of polarisabilities shown in Table 1.

The value of both $\langle p_{\parallel,rep}\rangle$ and $\langle p_{\perp,rep}\rangle$ shown in Fig. 9 for undeformed PET ($\lambda = 1$) is 189×10^{-25} cm^3. It can be seen that, due to the increasing alignment of the repeat units with the strain direction, and because $\beta_x^{ter} > \beta_y^{ter}$ and $\langle\beta_x^{gly}\rangle > \langle\beta_y^{gly}\rangle$, the values of $\langle p_{\parallel,rep}\rangle$ increase with increasing deformation, whilst the values of $\langle p_{\perp,rep}\rangle$ decrease. In accordance with Eqs. (41), (42), (49) and (50), the increases in $\langle p_{\parallel,rep}\rangle$ are greater in magnitude than the decreases in $\langle p_{\perp,rep}\rangle$. In addition, because [10,11,17,18] shorter chains become more aligned to the strain direction at smaller values of λ, the deviations from the undeformed value increase as chain length decreases. In the limit of complete alignment of all the chains, the values of $p_{\parallel,rep}$ and $p_{\perp,rep}$ given in Section 4 of Table 1 (230 and 162×10^{-25} cm^3, respectively) will be achieved.

Fig. 10 shows $\Delta\tilde{n}$ for PET chains of 60, 84, 108 and 150 bonds plotted versus $\lambda^2 - \lambda^{-1}$. The points have been

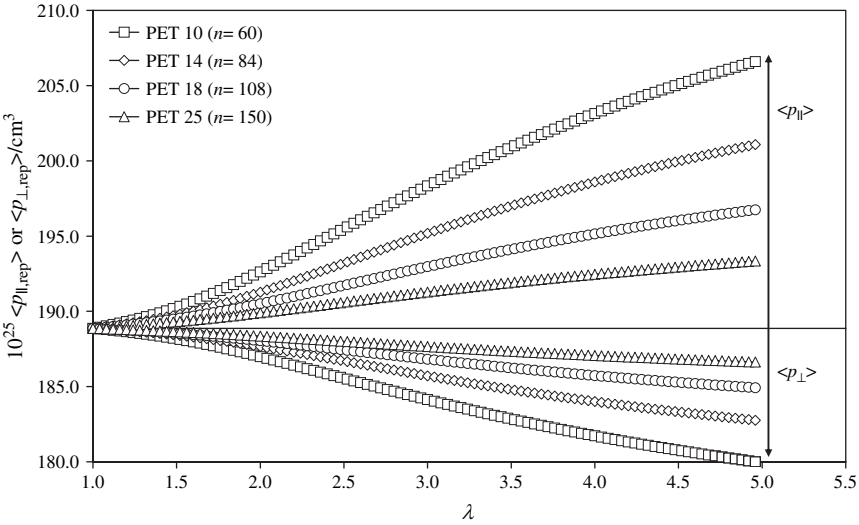

Fig. 9. $\langle p_{\parallel,rep}\rangle$ and $\langle p_{\perp,rep}\rangle$ versus λ for PET network chains of 60, 84, 108 and 150 bonds at 523 K based on Denbigh polarisabilities [22].

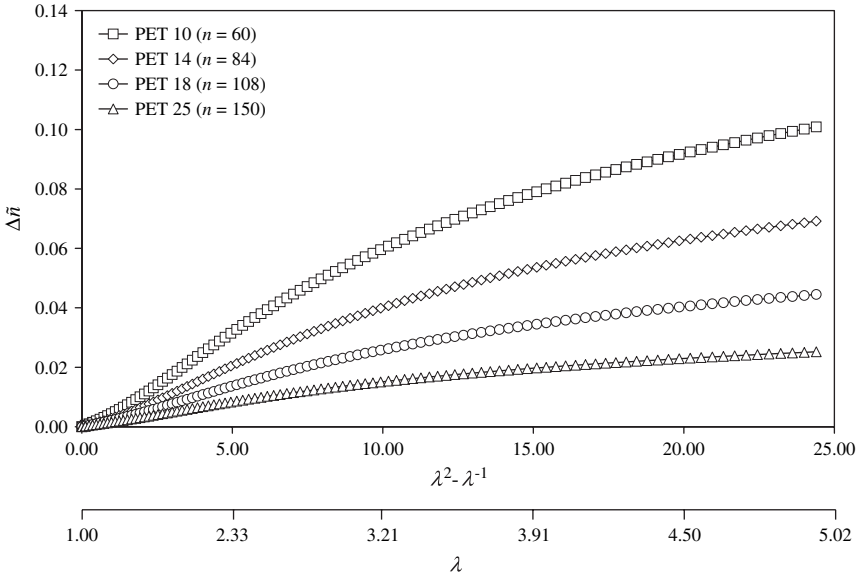

Fig. 10. Birefringence, $\Delta\tilde{n}$, versus $\lambda^2 - \lambda^{-1}$ for PET chains of 60, 84, 108 and 150 bonds at 523 K based on Denbigh polarisabilities [22].

calculated according to Eqs. (34) and (35), using the Denbigh bond polarisabilities and $\rho = 1.339\ \mathrm{g\,cm^{-3}}$ (see Paper I [9]). Use of the Bunn and Daubeny [21] or the LeGrand and Scacchetti bond polarisabilities again gives curves of a similar shape. At the highest extension shown ($\lambda \approx 5$), use of the Bunn and Daubeny bond polarisabilities gives values of $\Delta\tilde{n}$ about 10% lower than those shown in Fig. 10. On the other hand, use of the LeGrand and Scacchetti polarisabilities gives values of $\Delta\tilde{n}$ about 20% higher than those shown in Fig. 10 at the highest extension.

In Fig. 10, it can be seen that the shorter PET chains produce higher values of $\Delta\tilde{n}$ for a given deformation. This trend is again due to a greater proportion of the shorter chains becoming more aligned to the strain direction at smaller values of λ. $\Delta\tilde{n}$ may also be evaluated approximately using Eq. (37). The errors that arise at 500% strain are 1.49% for a chain of 10 repeat units and 0.34% for a chain of 25 repeat units. The limiting value, $\Delta\tilde{n}_{\max} = 0.262$, for perfectly aligned chains at large extensions shown in Table 1 is much larger than the values of $\Delta\tilde{n}$ in Fig. 10 at 500% extension.

Notice that, in disagreement with Kuhn and Grün theory, $\Delta\tilde{n}$ is not linearly related to $\lambda^2 - \lambda^{-1}$. Eq. (37) shows that, to a good approximation, $\Delta\tilde{n}$ is linearly related to $\langle p_{\parallel,\mathrm{rep}}\rangle - \langle p_{\perp,\mathrm{rep}}\rangle$ and Eqs. (39)–(42), (49) and (50) show that $\langle p_{\parallel,\mathrm{rep}}\rangle$ and $\langle p_{\perp,\mathrm{rep}}\rangle$ are linearly related to $\langle P_2(\cos\zeta_{\mathrm{ter}})\rangle$ and $\langle P_2(\cos\zeta_{\mathrm{gly}})\rangle$. Thus, the non-linear behaviour of $\Delta\tilde{n}$ with $\lambda^2 - \lambda^{-1}$ follows directly from the non-linear behaviour of $\langle P_2(\cos\zeta_{\mathrm{ter}})\rangle$ and $\langle P_2(\cos\zeta_{\mathrm{gly}})\rangle$ with that quantity. The non-linear behaviour of $\langle P_2(\cos\zeta_{\mathrm{ter}})\rangle$ with $\lambda^2 - \lambda^{-1}$ was confirmed experimentally in Paper I [9], and the measured values of $\langle P_2(\cos\zeta_{\mathrm{ter}})\rangle$ were found to be closely predicted by the present MC modelling.

The predicted values of $\Delta\tilde{n}$ will be used in Paper III [25] to model the measured birefringence of drawn PET.

Acknowledgements

The support of the EPSRC, access to the Accelrys Polymer software for the background RIS calculations, and the assistance of Anthony Appleyard (Manchester) with exact matrix algebra calculations for $\langle r^2\rangle$ are gratefully acknowledged. The useful discussions held with Dr. R.A. Jones (Leeds) are also gratefully acknowledged and the authors would like to thank Dr. E.L.V. Lewis for undertaking a survey of published bond-polarisability data.

References

[1] Kuhn W, Grun F. Kolloid Z 1942;101:248.
[2] Treloar LRG. The physics of rubber elasticity. 3rd ed. Oxford: Oxford University Press; 1975.
[3] Saunders DW. Trans Faraday Soc 1956;52:1425.
[4] Pinnock PR, Ward IM. Trans Faraday Soc 1966;62:1308.
[5] Nobbs JH, Bower DI, Ward IM. J Polym Sci Polym Phys Ed 1979;17:259.
[6] Nobbs JH, Bower DI. Polymer 1978;19:1100.
[7] Ward IM. Mechanical properties of solid polymers. Chichester: Wiley; 1971. p. 258.
[8] Kratky O. Kolloid Z 1933;64:213.
[9] Saunders LS, Ward IM, Cail JI, Stepto RFT. Polymer 2007;48:1360.
[10] Stepto RFT, Taylor DJR. Macromol Symp 1995;93:261.
[11] Stepto RFT, Taylor DJR. J Chem Soc Faraday Trans 1995;91:2639.
[12] Taylor DJR, Stepto RFT, Jones RA, Ward IM. Macromolecules 1999; 32:1978.
[13] Cail JI, Taylor DJR, Stepto RFT, Brereton MG, Jones RA, Ries ME, et al. Macromolecules 2000;33:4966.
[14] Pinnock PR, Ward IM. Br J Appl Phys 1964;15:1559.
[15] Kashiwagi M, Cunningham A, Manuel AJ, Ward IM. Polymer 1973; 14:111.
[16] Cail JI, Stepto RFT, Taylor DJR, Jones RA, Ward IM. Phys Chem Chem Phys 2000;2:4361.
[17] Cail JI, Stepto RFT. Polymer 2003;44:6077.
[18] Saunders LS, Ward IM, Cail JI, Stepto RFT. Polymer 2004;45:2357.
[19] Williams AD, Flory PJ. J Polym Sci 1967;5(A2):417.

[20] Volkenstein MV. High polymers. In: Timasheff SN, Timasheff MJ, editors. Configurational statistics of polymeric materials, vol. XVII. New York: Wiley Interscience; 1963. English trans [chapter 7].
[21] Bunn CW, Daubeny R de P. Trans Faraday Soc 1954;50:1173.
[22] Denbigh KG. Trans Faraday Soc 1940;36:936.
[23] LeGrand DG, Scacchetti PA. Intrinsic birefringence of polymers. GE Global Research, <http://www.crd.ge.com/cooltechnologies/pdf/1999069.pdf>; 1999 [accessed 29.08.99].
[24] Ward IM, Bleackley M, Taylor DJR, Cail JI, Stepto RFT. Polym Eng Sci 1999;39:2335.
[25] Cail JI, Saunders LS, Stepto RFT, Ward IM. Polymer 2007;48:1379.
[26] Flory PJ. Statistical mechanics of chain molecules. New York: Wiley Interscience; 1969.
[27] Ward IM. Adv Polym Sci 1985;66:81.
[28] Ward IM. Proc Phys Soc 1962;80:1176.